ACS Partner Journal

CHEM & BIO ENGINEERING

pubs.acs.org/ChemBioEng

Article

Bioinspired DNA Plastics with Brick-and-Mortar Structure: Enhanced Toughness, Recyclability, and Degradability

Xiaofeng Li, Xi Shan, Jiadong Chen, Jun Zhu, Yang Chen, Xueyi Chen, Shahao Li, Mengze Lu, Yuhui Du, Panchao Yin, Tingjian Chen,* and Taolin Sun*

Cite This: *Chem Bio Eng.* 2025, 2, 303−311

Read Online

ACCESS | Metrics & More | Article Recommendations | Supporting Information

ABSTRACT: Bio-based plastics offer the advantage of biodegradability over traditional petroleum-based plastics, enabling natural reintegration into the environment and positioning them as a more sustainable alternative. DNA, as a natural biopolymer, exhibits excellent biocompatibility and degradability. However, the mechanical strength of currently biomass DNA-based materials is inferior to that of other bio-based and petroleum-based plastics. In this work, DNA plastics with a "brick-and-mortar" structure were fabricated using DNA extracted from onions through bidirectional freezing, water vapor annealing, and compression densification. This biomimetic design significantly enhances the fracture toughness (~1.5 MPa·m$^{1/2}$) while possessing a high elastic modulus (~560 MPa) of DNA plastic, making it superior or comparable to existing bio-based plastics and petroleum-based plastics, and thus positioning it as a potential structural material. Analysis of crack propagation behavior in DNA plastics reveals that their high toughness stems from a hierarchical "brick-and-mortar" structure operating across multiple length scales, facilitating a multiscale fracture process from macroscopic to molecular levels. Furthermore, these DNA plastics can be efficiently recycled in aqueous environments and fully biodegraded by enzymes, demonstrating strong environmental friendliness and significant potential for sustainable development.

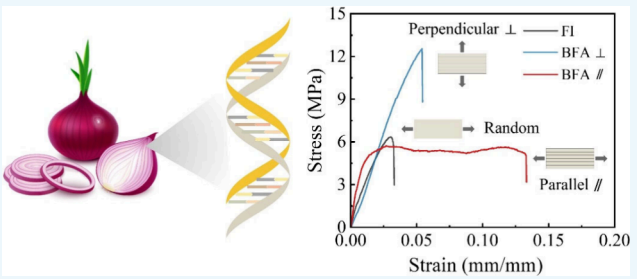

KEYWORDS: *DNA plastics, Bidirectional freezing, Brick-and-mortar, Toughness, Degradable plastics*

INTRODUCTION

Petroleum-based plastics, derived from raw petroleum materials, are extensively utilized across various industries, including packaging, electronics, automotive, aerospace, and medical fields.[1−5] However, their widespread use poses significant challenges, such as environmental pollution, resource depletion, microplastic contamination, and greenhouse gas emissions.[6,7] Consequently, the development of sustainable alternatives has become increasingly urgent. Biodegradable, recyclable plastics derived from sustainable resources are viewed as promising solutions to mitigate environmental and resource-related pressures.[8,9] These innovative materials are steering the plastics industry toward a more sustainable and ecofriendly future, with the potential to address the current issues. Significant advancements have already been achieved in the development of bio-based biodegradable plastics produced from starch, cellulose, and polysaccharides.[10−12] In addition, DNA, the core genetic material in living organisms, is widely abundant in plants, animals, and microorganisms. The unique biological and chemical properties of DNA, along with its programmability and biodegradability, make it an attractive candidate for developing sustainable materials. Current research on DNA-based materials mainly focuses on functional modifications to create hydrogels, hybridizing with polymers or inorganic fillers to form composite materials, or producing bioplastics through chemical cross-linking.[13−16] Despite these significant advancements in DNA plastics, they remain limited in their mechanical brittleness and weakness, with a relatively low modulus (21 MPa) and fracture tensile strength (2.5 MPa).[13] This performance is considerably inferior to other bio-based and petroleum-based plastics, preventing them from being considered suitable for use as engineering structural materials.

Natural materials like nacre and bone exhibit remarkable fracture tolerance while maintaining their rigidity.[17,18] Issues related to crack propagation in these biominerals can be mitigated through mechanisms, such as crack bridging, deflection, and branching. Investigations on these toughness mechanisms reveal that these materials have hierarchical structures with multiple structure length scales. This multiscale structure facilitates a fracture process that spans from

Received: December 30, 2024
Revised: February 24, 2025
Accepted: March 5, 2025
Published: March 14, 2025

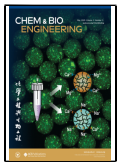

https://doi.org/10.1021/cbe.4c00190
Chem Bio Eng. 2025, 2, 303−311

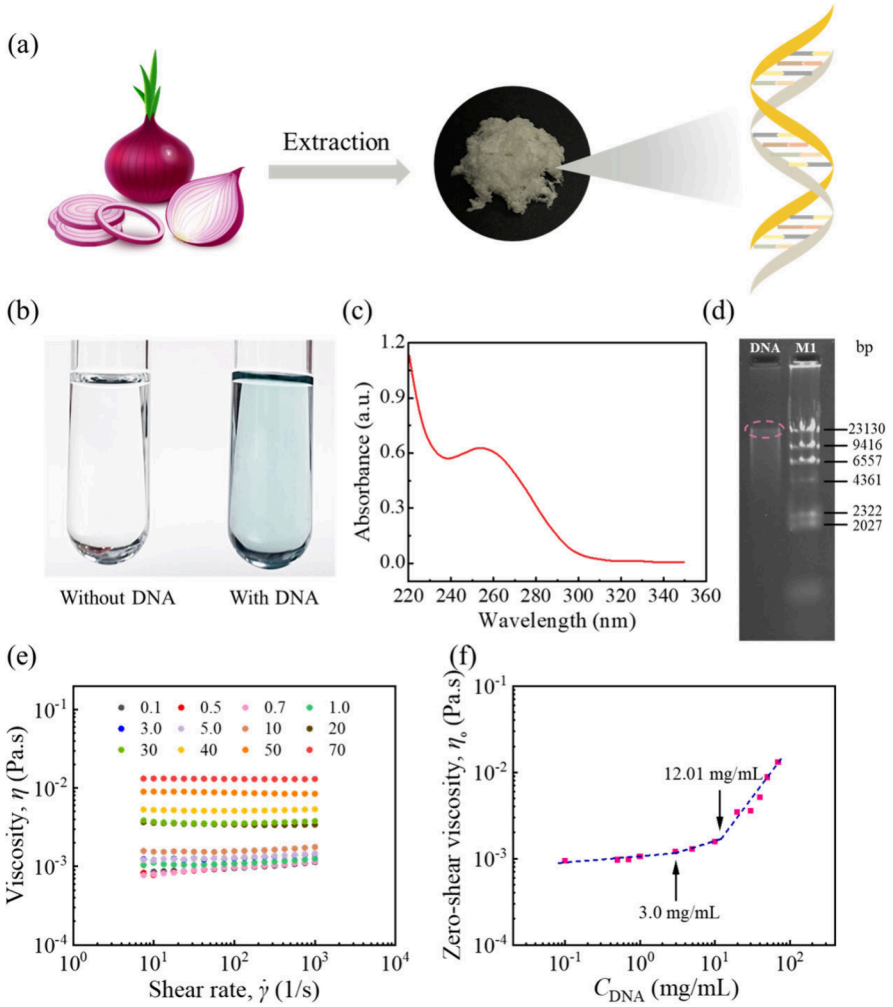

Figure 1. Extraction and characterization of DNA from onions. (a) Schematic diagram of the DNA extraction process from onions. (b) Diphenylamine method for identification of the presence of DNA. (c) UV absorption spectra of DNA solutions. (d) Gel electrophoresis bands of DNA molecules with standard samples for estimating the molecular weight measurement of DNA. "M1" represents the molecular weight of marker-Gene Ruler 23 kb DNA ladder. (e) Dependence of the viscosity of DNA solutions at different concentrations on the shear rate. (f) η_0 of DNA solutions at different concentrations C_{DNA}.

macroscopic to molecular levels, effectively diminishing stress concentrations at crack tips and slowing crack propagation. Numerous strategies are employed to fabricate materials with hierarchical structures that mimic the complex architectures found in natural materials, including phase separation, magnetic fields, electric fields, and others. Among these, the ice-templating method is distinguished by its scalability, versatility, and cost-effectiveness, effectively producing tough and stiff hydrogels and composite materials utilizing both synthetic polymers and biopolymers.[18,19]

In this study, inspired by the hierarchical structures of biomaterials, we developed tough and stiff DNA plastics with multiscale architectures through an ice-templating method combined with a thermal annealing process. This approach facilitates the formation of "brick-and-mortar" organized lamellar structures at the microscale and establishes the strong bonding between DNA chains, including hydrogen bonding and π-π interactions at the nanoscale. As a result, the DNA plastic exhibits a high stiffness of approximately 560 MPa, fracture stress of around 5.2 MPa, and toughness of about 3.78 kJ/m^2. By extracting DNA in bulk from onions, we efficiently and cost-effectively converted biomass DNA into durable plastic on a large scale. Additionally, DNA plastic demonstrates effective recyclability in aqueous environments and complete biodegradability under enzymatic conditions, highlighting its excellent environmental sustainability.

RESULTS AND DISCUSSION

Extraction and Characterization of DNA. To create DNA plastics as the structure materials, employing efficient and cost-effective methods for mass scale DNA extracted from diverse biological sources is essential. Onions were selected as the raw material for DNA extraction due to their high cellular nucleus content, large cell volumes, and cost-effectiveness, thereby improving extraction efficiency. Furthermore, in comparison, animal DNA tends to contain higher levels of protein contaminants, while microbial DNA requires more complex purification procedures. Here, we employed a cetyltrimethylammonium bromide (CTAB) method with modifications to extract DNA from onions on a bulk scale,[20] encompassing a series of steps including freezing and grinding, extraction, centrifugation, precipitation, and washing, which yielded grams of DNA powders (Figure 1a). To verify the presence of DNA in the extracted product, the diphenylamine

https://doi.org/10.1021/cbe.4c00190
Chem Bio Eng. 2025, 2, 303−311

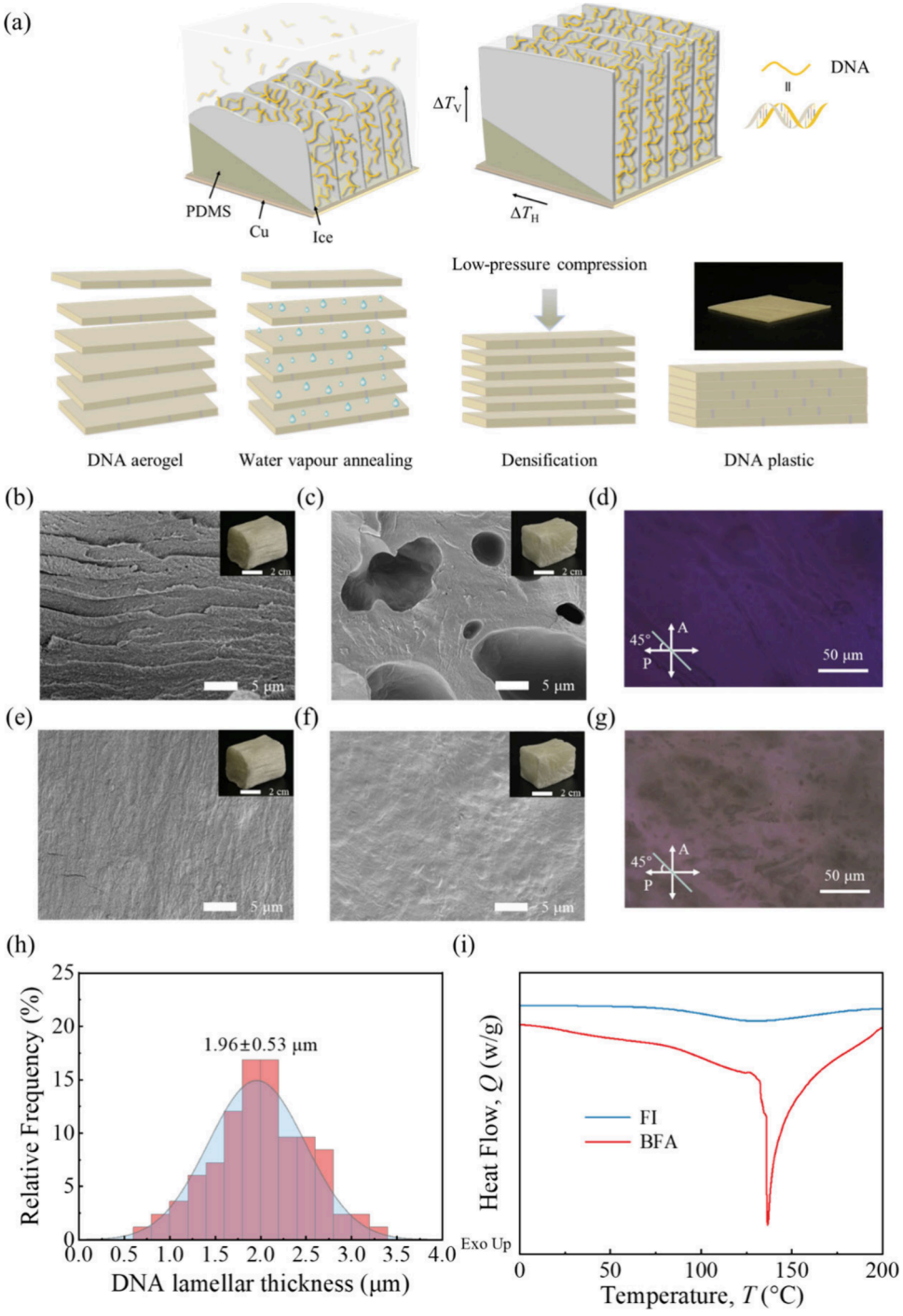

Figure 2. Fabrication and characterization of DNA plastics. (a) Schematic process for the preparation of DNA plastics BFA. Cross section (C) morphology of DNA plastic BFA (b) and FI (c) by SEM. Section (S) morphology of DNA plastic BFA (e) and FI (f) by SEM. Inset figures represent the corresponding morphology of DNA aerogels. Optical morphology of DNA plastics BFA (d) and FI (g) under the crossed polarizers at 45°, where the polarizer (P) is perpendicular to the analyzer (A). (h) Thickness statistics of the lamellar structure in BFA cross-section. (i) DSC curves of DNA plastics BFA and FI.

method was employed.[21] This method involves a reaction between diphenylamine and DNA in an acidic environment, yielding a blue conjugated product. After adding the extract to the system and allowing it to react, the system turned blue, while the control without the extract remained clear and transparent (Figure 1b). This indicates the presence of DNA in our extracted product. To quantify the DNA content in the extracted product, UV absorbance spectroscopy was performed (Figure 1c). Absorbance at 260, 280, and 230 nm was measured to represent nucleic acids, proteins, and other contaminants (such as carbohydrates, phenol or guanidine HCl), respectively. An A260/A280 ratio of 2.05 is higher than the typical value of ∼1.8 for pure DNA.[22] This suggests that the DNA sample may have undergone some degradation or may contain small fragments and single-stranded DNA. Furthermore, an A260/A230 ratio of 0.89 is significantly lower than the typical range of 1.8 to 2.2 for pure DNA. The measured A260/A280 and A260/A230 ratios both indicate the

https://doi.org/10.1021/cbe.4c00190
Chem Bio Eng. 2025, 2, 303−311

impurity of the extracted DNA. The estimated DNA concentration was determined to be approximately 28 ng/μL.

We further utilized agarose gel electrophoresis to estimate the molecular weight of DNA extracted from onions. As a polyelectrolyte, DNA migrates through the porous agarose gel under the influence of an electric field. The migration speed of DNA fragments varies depending on their size, enabling the separation of these fragments. By comparing the migration distances of DNA fragments to the standard M1 (Figure 1d), the number-average molecular weight of DNA is roughly estimated as 0.14×10^8 g/mol. Due to the long chain as well as the polyelectrolyte nature of DNA, the variations in the concentration can impact their chain conformation, leading to their specific rheological behavior. The shear flow test was performed to investigate the rheological properties of DNA solutions with various concentrations of C_{DNA} ranging from 0.1 to 70 mg/mL, as shown in Figure 1e. It was found that the viscosity η of the DNA solution is independent of the changes in shear rate in the investigated range of C_{DNA}, indicating the Newtonian fluid characteristic. We summarized their zero-shear viscosity (η_0) against C_{DNA}, where η_0 is determined from η at a low shear rate (~7 1/s). Figure 1f shows that η_0 increases with C_{DNA}, and three regions were observed according to C_{DNA} range. In the dilute solution region (C_{DNA} < 3 mg/mL), DNA chains are primarily isolated, with η_0 linearly increase with C_{DNA}. As the concentration increases, the solution transitions from the dilute to the semidilute region (3 mg/mL < C_{DNA} < 12.01 mg/mL). DNA chains begin to interact and overlap, leading to a noticeable increase in viscosity, following the scaling relation $\eta_0 \sim C_{DNA}^{0.3}$. At the high concentration regions, viscosity increases rapidly as DNA chains are entangled, along with the increased inter- and intraactions, following another scaling relation $\eta_0 \sim C_{DNA}^{1.3}$. From this observation, we estimated the crossover points for the overlap concentration C^* (=3 mg/mL), and the entanglement concentration C_e (=12.01 mg/mL) using these two scaling relations. Based on the rheological results, a 30 mg/mL DNA higher than C_e was selected as the precursor solution for fabricating DNA plastics as the high level of entanglement of the DNA chains at this concentration enhances the structural stability and toughness.

Fabrication of DNA Plastic. Bidirectional freezing, as a controlled, versatile, scalable, and environmentally friendly method, was used to create nacre-like ordered structures of DNA plastic by establishing dual temperature gradients, making it a powerful tool for enhancing the macroscopic properties.[23−26] The nacre-like structure of DNA plastics was synthesized using a combination of bidirectional freezing, water vapor annealing, and compression densification techniques (Figure 2a). Initially, a 30 mg/mL DNA aqueous solution was injected into a polydimethylsiloxane (PDMS) mold designed for bidirectional freezing. Upon freezing, the low thermal conductivity of PDMS initiated cooling in the wedge-shaped region at the bottom of the mold, facilitating ice crystal formation. The vertical (ΔT_V) and horizontal (ΔT_H) temperature gradients encouraged preferential outward growth of ice crystals along the cold front and horizontal growth along the PDMS wedge. This unique freezing mechanism enables the self-orientation of DNA chains. As the ice crystals advance, DNA molecules are pushed into the interstitial spaces between the crystals, resulting in a lamellar structure described as "bricks". These layers align along the direction of the ice template, with each lamellar layer of 1.96 μm in thickness. A sample with a thickness of 1.27 mm comprises approximately 650 layers (Figure 2h). During the subsequent lyophilization process, the three-dimensional DNA network was preserved after ice sublimation through chain entanglements and interactions between the double helices. This results in a DNA aerogel with a characteristic long-range lamellar structure. The aerogel further undergoes water vapor annealing, allowing water to infiltrate the aerogel and plastify the surface of the lamellar layer. These plasticized DNA chains then form a "mortar" on the lamellar surfaces. In the compression densification stage, the "mortar" and "bricks" adhere tightly through adhesive interactions between the DNA lamellae, ultimately yielding a lamellar biomimetic DNA plastic with a "brick-and-mortar" architecture, referred as BFA. The cross-sectional microstructure is shown in Figure 2b and closely resembles natural nacre, showing a distinct long-range lamellar structure with anisotropic features. The sectional microstructure also arranges in the same direction (Figure 2e). In contrast, isotropic DNA plastics (referred to as FI), prepared using conventional freezing methods, typically display random ice crystal growth, resulting in a nonuniform porous structure in the cross-section and nonconventional structure in the section (Figure 2c and f).

To verify the anisotropic and isotropic properties of the DNA plastics, polarized light microscopy was performed. Anisotropic DNA plastics BFA exhibit strong birefringence, evidenced by shifts in interference colors or brightness when the sample was rotated at 45° under crossed polarizers (Figures 2d and S1), and thus confirm the uniaxially ordered plastic. In contrast, isotropic DNA plastic FI does not exhibit such birefringent properties (as depicted in Figures 2g and S1). Figure 2i presents the differential scanning calorimetry curves of DNA plastics with anisotropic and isotropic structures. Both samples exhibit a similar glassy transition temperature around 100 °C. However, in comparison to isotropic DNA plastics FI, the anisotropic DNA plastics BFA display a melting peak around 135 °C, indicating the presence of a crystalline structure. Wide-Angle X-ray Scattering (WAXS) also revealed that the DNA FI are amorphous, while scattering peaks were observed within DNA plastics BFA (Figure S2), which is consistent with the results by DSC. The intensity differences of diffraction peaks shown in the cross-section and section of the anisotropic sample (BFA) reflect the degree of crystallinity resulting from the layered arrangement. In order to identify and confirm the presence of functional groups, we use Fourier transform infrared (FTIR) spectroscopy to provide insights into the interactions within the DNA plastic. Figure S3 presents the FTIR spectra of DNA powders, DNA plastics BFA, and FI within the range 3500−800 cm^{-1}. The peak around 1600 cm^{-1}, attributed to the stretching vibrations of the nitrogen−hydrogen bond (−N-H) in DNA powders, shifts to a higher wavenumber (~1615 cm^{-1}) in DNA plastics BFA and FI. This shift indicates a decrease in the strength of hydrogen bonding between the base pairs of DNA chains, suggesting that the freezing process, including both conventional and bidirectional methods, may disrupt the double helix structure of DNA through hydrogen bonds. However, compared to DNA powders, a peak around 3038 cm^{-1}, attributed to the stretching vibrations of unsaturated carbon−hydrogen bonds (C−H) of the aromatic ring on the base pairs, becomes more pronounced in DNA plastics FI and even stronger in DNA plastics BFA. This suggests that the freezing process reduces the flexibility of DNA strands, making the base

https://doi.org/10.1021/cbe.4c00190
Chem Bio Eng. 2025, 2, 303−311

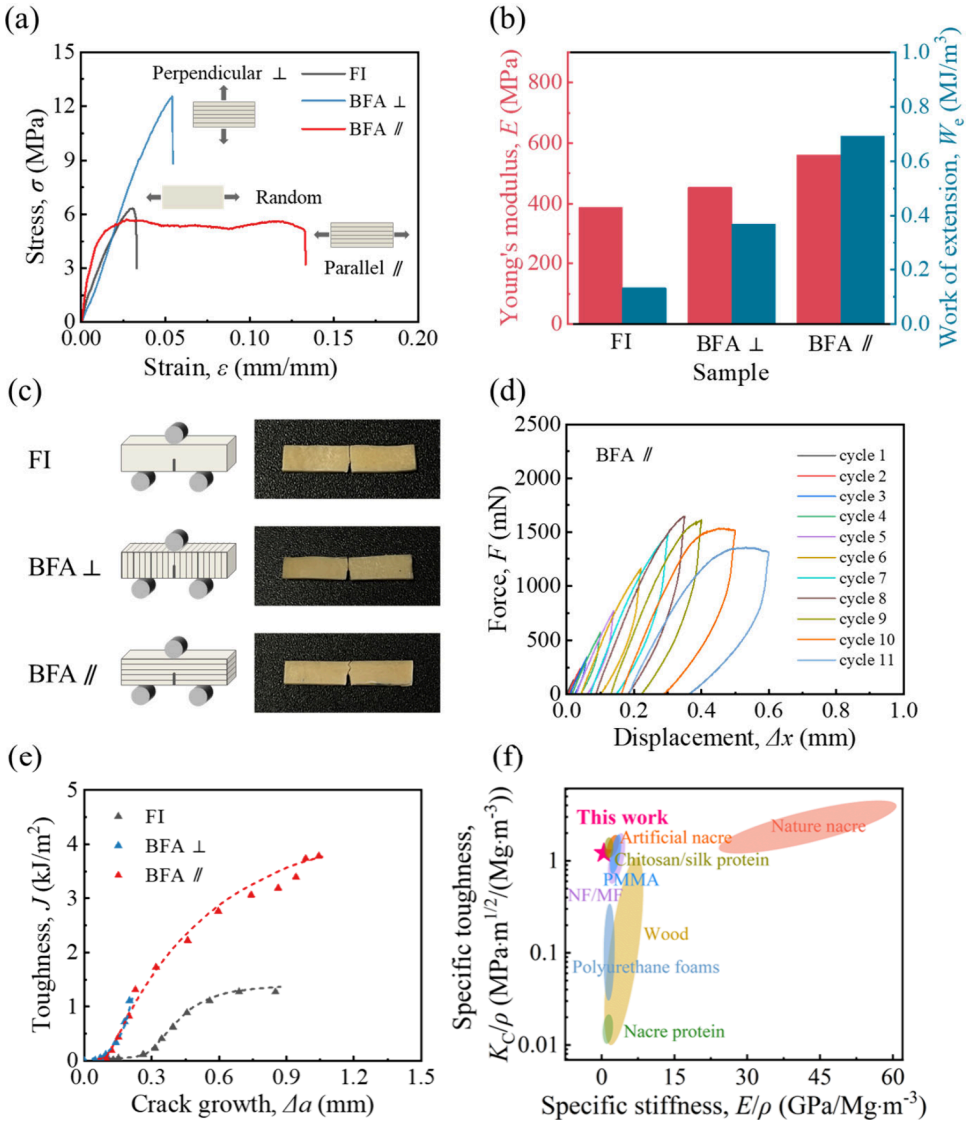

Figure 3. Mechanical properties of DNA plastics. (a) Uniaxial tensile stress−strain curves of anisotropic and isotropic DNA plastics (FI, BFA ⊥ and BFA ||). (b) Young's modulus (E) and work of extension (W_e) of DNA plastics (BFA ⊥, BFA || and FI). (c) Schematic of SENB test and optical photographs of DNA plastics (FI, BFA ⊥ and BFA ||) following fracture. (d) Result curves of DNA plastic BFA || by cyclic loading−unloading experiments specimens. (e) Comparison curves for toughness (J) as functions of crack extension length for anisotropic and isotropic DNA plastics (FI, BFA ⊥ and BFA ||). (f) Ashby diagram of specific toughness versus specific stiffness for DNA plastic compared with different natural and artificial materials, including nacre protein,[25] nature nacre,[27] NF/MF (microfiber/nanofiber),[28] artificial nacre,[27] chitosan/silk protein,[17] poly(methyl methacrylate),[29] wood[30] and polyurethane foams.[31]

pairs more rigid and less prone to movement in DNA plastics FI. Moreover, the bidirectional freezing process induces a more ordered arrangement of DNA strands, leading to the formation of a more compact structure in DNA plastics BFA. The enhanced peak intensity can be attributed to the strengthening of π-π interactions between the base pairs. The bidirectional freezing process likely promotes a more ordered arrangement of DNA strands, enhancing π-π stacking interactions between the base pairs, which contribute to the overall stability and structural integrity of the DNA molecule.

Rigid Yet Toughness of DNA Plastic. A tensile test was conducted to compare the mechanical behavior of DNA plastics with anisotropic (BFA) and isotropic (FI) structures, with the loading direction applied vertically (BFA ⊥) and parallel (BFA ||) to the direction of ice crystal growth for the former sample. As shown in Figure 3a, the mechanical response of the isotropic DNA plastic FI is linearly elastic and exhibits brittle characteristics, with a fracture strain of 3% and a fracture stress of 6.3 MPa. In contrast, the anisotropic plastic BFA displays distinct mechanical properties: the BFA ⊥ samples demonstrate brittle fracture, with a low fracture strain of 5% and fracture stress of 12.5 MPa, whereas the BFA || samples show an increase in stress with strain up to a maximum point, followed by plastic flow, where the stress remains nearly constant as the strain increases, until the sample fractures at high deformation with a fracture strain of 13% and fracture stress of 5.2 MPa. The BFA || samples exhibit remarkable fracture tolerance with a high work of extension (~0.7 MJ/m^3) while maintaining their rigidity (~560 MPa), compared to the BFA ⊥ samples (0.37 MJ/m^3 and 453 MPa) and the FI samples (0.13 MJ/m^3 and 387 MPa) (Figure 3b). The superior mechanical performance of anisotropic DNA

https://doi.org/10.1021/cbe.4c00190
Chem Bio Eng. 2025, 2, 303−311

plastics is due to their hierarchical "brick-and-mortar" structure, which operates across multiple length scales. When a load is applied, force is transmitted through the brick layers and shearing occurs in the mortar between them. This brick sliding mechanism is crucial for enhancing plasticity at this scale, dissipating significant mechanical energy to toughen the material.

To further evaluate the toughness of DNA plastics, a three-point single-edge-notched bending (SENB) test was performed on the notched BFA and FI samples with a precut length of 1.5 mm. For the BFA sample, the direction of precut length was applied both parallel (BFA ⊥) and vertical (BFA ∥) to the direction of ice crystal growth, with the loading direction positioned vertically on the surface of the sample (Figure 3c). DNA plastics underwent cyclic loading and unloading at specified displacements (Δx), followed by additional cycles at higher displacements, until complete fracture propagation was achieved. As shown in Figure 3d and S4, at low applied displacements, the force−displacement curves for all samples (FI, BFA ⊥, and BFA ∥) exhibited linear growth and returned to the initial state upon unloading without hysteresis, indicating they remained in the linear elastic region. As displacement increased, the presence of hysteresis loops indicated plastic flow, with the BFA ⊥ sample displaying significantly larger hysteresis than both BFA ∥ and FI. Notably, the hysteresis of the BFA ∥ sample was much lower than that of the FI sample. The fracture morphologies indicated that FI and BFA ⊥ specimens displayed nearly planar extension paths, indicating brittle fractures (see Figure 3c; Movies S1 and S2). In contrast, the BFA ∥ sample exhibited a distinct sawtooth fracture pattern, highlighting the effectiveness of its hierarchical "brick-and-mortar" structure in energy dissipation and crack resistance (see Figure 3c; Movie S3). These results suggest that in the case of BFA ⊥, when a load is applied, force is transmitted through the brick layers, leading to shear in the mortar between them. When the crack encounters the lamella layers, propagation requires not only breaking the tightly bound DNA chains within the lamella layers at the microscale but also overcoming the strong interfaces between the lamella layers at the molecular scale, which are stabilized by hydrogen bonding and π-π interactions among the DNA helix chains. This significantly dissipates the mechanical energy and inhibits crack propagation. In BFA ⊥, the crack direction aligns with the lamella layers, making it easier for cracks to occur at the interfaces between brick layers. As a result, brick sliding dominates, requiring less energy to fracture the BFA ⊥ sample compared to the BFA ∥ and FI samples. The fracture process of three samples results in the formation of crack propagation process zone ahead of the crack tip, and thus the total energy required to crack the sample J can be commonly divided into elastic (J_{el}) and plastic (J_{pl}) contributions, similar to the analysis in other biological materials such as bone.[19,32−37] The elastic contribution primarily arises from the fracture of the DNA chains, while the plastic contribution is attributed to viscoelastic or viscoplastic energy dissipation around the crack tip, including the sliding of DNA layers and the breaking of hydrogen bonds or π-π stacking interactions. The resulting crack resistance curve (J curve) of toughness (J) dependence of crack growth length (Δa) is shown in Figure 3e for the three samples. Both J_{el} and J_{pl} increase with Δa, with J_{pl} significantly exceeding J_{el}. Notably, J_{pl} in BFA ∥ is considerably higher than that in FI and BFA ⊥, indicating that the layered structure effectively hinders crack propagation (Figure S5). Therefore, crack growth of the J curve reaches 3.78 kJ/m^2 in BFA ∥, approximately three times that of FI (1.27 kJ/m^2) (Figures 3e and S5), underscoring the crucial role of its complex multiscale structure in enhancing toughness. Under sustained loading, this architecture promotes crack branching and microcrack formation, complicating the propagation path ahead of the crack tip. As cracks traverse the layers, they encounter significant energy barriers, resulting in preferential deflection and redirection along the DNA layer interfaces. This process involves mechanisms such as sliding, pullout, abrasion, and fracture of the DNA layers, all requiring additional energy dissipation.

Our DNA plastics exhibit high fracture toughness despite their rigidity, as highlighted in Figure 3f which compares the specific toughness K_C/ρ, defined as the ratio of fracture toughness K_C per mass density ρ, and specific stiffness with reported bionic materials, synthetic plastics in literatures and our DNA plastics, where K_C was related to the modulus E and J, which was calculated in SI. It is shown that DNA plastics outperform existing synthetic plastics and natural materials, such as nacre protein,[25] wood[30] and polyurethane foams.[31] At the same time, benefiting from the brick-and-mortar structure, nacre-like DNA plastics achieve a performance level comparable to artificial nacre,[27] NF/MF,[28] and is on par with chitosan/silk protein[17] and poly(methyl methacrylate),[29] indicating a promising potential for application.

Recyclability and Biodegradability of DNA Plastics. Despite its high stiffness and toughness, DNA plastics can be recycled based on their features. As illustrated in Figure 4a, DNA plastic can be transformed back into a DNA solution by weakening the hydrogen bonds within its pearl-layer structure with water. This solution can then be reprocessed into layered DNA plastic through freeze-drying, dissolution, and bidirectional freezing, thereby completing a closed-loop recycling process. Moreover, due to the inherent properties of DNA, DNA plastics are fully biodegradable. Under the action of DNase I, the enzyme's active site recognizes and catalyzes the hydrolysis of DNA, leading to the cleavage of DNA chains. As shown in Figure 4c, DNA plastics can be completely biodegraded within 8 h. The blurring and reduction in the intensity of DNA gel electrophoresis bands after degradation, as depicted in Figure 4b, further illustrate the excellent biodegradability of DNA plastics, underscoring their potential as a sustainable material.

CONCLUSION

In summary, we successfully extracted DNA from onions with a molecular weight of approximately 10^8 g/mol. Rheological testing indicated that the DNA solution exhibits Newtonian fluid characteristics. Additionally, we constructed DNA plastics with a "brick-and-mortar" multiscale structure using bidirectional freezing technology. In comparison to isotropic DNA plastics, the anisotropic structure endowed the DNA plastics with a higher modulus (560 MPa) and increased fracture toughness (~1.5 MPa·m$^{1/2}$). SENB tests revealed that the high toughness originates from plastic dissipation at the crack tip. Furthermore, these DNA plastics demonstrated excellent recyclability and complete biodegradability. This work systematically explores the relationship between the mechanical properties and structure of DNA materials, laying a solid foundation for the development of high-performance materials. Furthermore, the developed DNA plastics can serve as sustainable substrates for flexible electronics, including 3D

https://doi.org/10.1021/cbe.4c00190
Chem Bio Eng. 2025, 2, 303−311

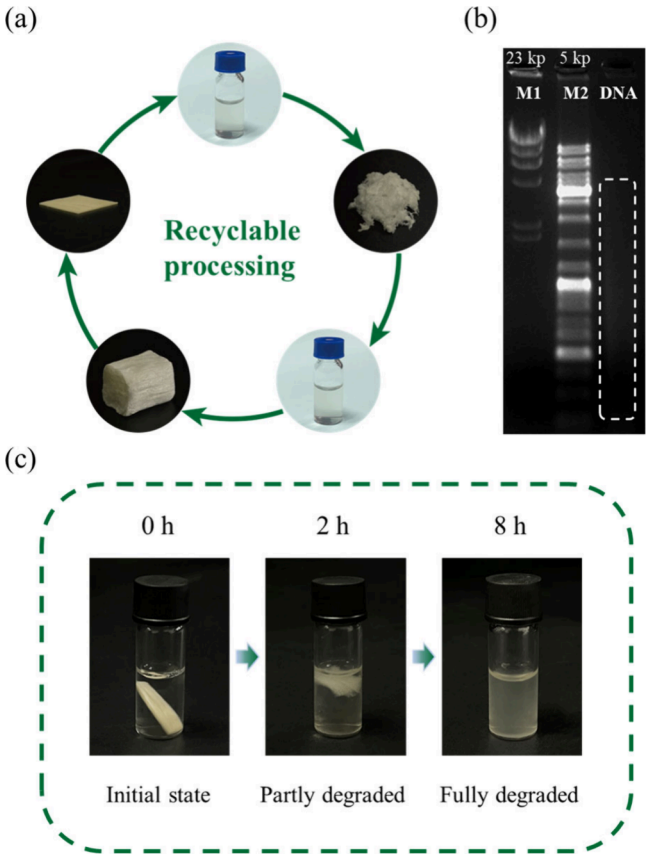

Figure 4. Recyclability and biodegradability of DNA plastics. (a) Schematic of the recyclability of DNA plastics. (b) Gel electrophoresis bands of DNA plastics after complete biodegradation. "M1" and "M2" represent molecular weight markers, Gene Ruler 23 and 5 kb DNA ladder, respectively. (c) Optical photographs of morphological changes at different time points during the degradation of DNA plastics.

printing materials, biodegradable circuit board insulation layers, and sensor substrates.

EXPERIMENTAL SECTION

Materials. Fresh onions were used for the deviation of DNA. 2-Mercaptoethanol and Agarose were purchased from TCI Chemical Trading Co., Ltd. (Shanghai). 2*CTAB extraction buffer was purchased from Shanghai Acmec Biochemical Technology Co., Ltd. Chloroform and sulfuric acid were purchased from Chengdu Kelong Chemical Co., Ltd. 3-Methyl-1-butanol, ethanol, acetic acid and acetaldehyde were purchased from Beijing InnoChem Science & Technology Co., Ltd. Diphenylamine was purchased from Shanghai Titan Scientific Co., Ltd. PDMS (SYLGARD 184) was purchased from Dow Corning Co., Ltd. To fabricate a bidirectional freezing mold, the PDMS precursor solution was poured into a PMMA mold (20 × 20 × 30 mm), the bottom of the mold was sealed with a copper plate with a tilt angle of 20°, and the PDMS wedge was obtained by curing for more than 12 h at room temperature.

DNA Extraction Procedure. DNA was extracted from onions according to the previous work.[18] CTAB buffer solution (250 mL) was preheated to 65 °C, and 2-mercaptoethanol (10 mL) was added and thoroughly mixed. Onions were quickly frozen in liquid nitrogen at −196 °C and ground into a fine powder using a sterile mortar. The ground onion powder (250 g) was added to the preheated mixture and gently mixed, followed by incubation in a water bath for 45 min. Subsequently, the mixture was cooled to room temperature, and an equal volume of chloroform alcohol (24:1, v/v) was added. The mixture was inverted several times and then centrifuged at 12,000 rpm for 10 min. The supernatant was collected, and this step was repeated twice. The collected supernatant was precipitated by the addition of cold anhydrous ethanol. After overnight incubation, the mixture was centrifuged at 5,000 rpm for 5 min to recover the white flocculent DNA precipitate. The precipitate was then washed with anhydrous ethanol and 75% ethanol. After being dried, the DNA was stored at −20 °C for further use.

Fabrication of DNA Plastic. First, DNA solution (3%, w/v) was injected into a bidirectional freezing mold composed of a PDMS wedge, which was placed on a copper plate with half of the plate immersed in liquid nitrogen. After being frozen, the sample was removed from the mold and freeze-dried at 5 Pa and −80 °C for 48 h to obtain DNA aerogels. To fabricate DNA plastics with a nacre-like structure, the freeze-dried DNA aerogels were subjected to water vapor annealing in a sealed environment with 70% relative humidity. Subsequently, the aerogels were vertically compressed using a hot press at room temperature under a pressure of approximately 10 MPa for 40 min, resulting in anisotropic DNA plastics. When the DNA solution was injected into a mold without PDMS for freezing, followed by the same freeze-drying, annealing, and compression procedures, isotropic DNA plastics were produced.

Characterization. *Rheological Measurement.* The rheological properties of the DNA solution were evaluated by using an ARES-G2 rheometer equipped with a DIN concentric cylinder setup. Steady-state shear experiments were performed across a shear rate range of 0.1 s^{-1} to 1000 s^{-1} at the room temperature.

Micro-spectrophotometer (MSP). Quantitative analysis of biomass DNA extracted from onions was conducted by using a microvolume spectrophotometer (Nano-300). Following instrument calibration, a DNA sample (1−2 μL) was placed on the measurement platform for detection. The A260/A280 ratio and DNA concentration were subsequently measured and recorded.

Agarose Gel Electrophoresis (AGE). The number of DNA base pairs was determined using agarose gel electrophoresis. The DNA sample along with a DNA marker was loaded into the wells of the agarose gel. An electric field was applied to separate the DNA fragments based on size. Following electrophoresis, the DNA band was visualized using an imaging system (Gel/View 5000 Pro). The size of the band was then compared with the DNA marker of known size to determine the number of base pairs in the sample.

Scanning Electron Microscopy (SEM). The microstructure of the cross sections of DNA plastics was characterized by using a scanning electron microscope (JEOL JSM-7900F, Japan). DNA plastics were cryogenically fractured in liquid nitrogen, followed by gold sputtering, using a sputter coater. The samples were then observed in the chamber with an electron beam accelerating voltage of 15 kV.

Polarized Light Microscopy (POM). The DNA samples were placed in the center of a slide under a polarized light microscope (Leica DMP4). The sample orientation was examined, and corresponding images were captured at 50× magnification in polarized bright-field mode.

Differential Scanning Calorimetry (DSC). Differential scanning calorimetry (DSC) measurements were performed by using a TA DSC2500 instrument. The samples were first heated from room temperature to 100 °C at a rate of 10 °C/min under a nitrogen atmosphere to eliminate the thermal history and then reheated at a heating rate of 5 °C/min over the range of 0 to 200 °C.

Tensile Testing. The mechanical properties of the DNA plastics were evaluated using a universal testing machine (Instron 5965, USA). A 100 N sensor was employed, and uniaxial tensile tests were performed at a rate of 10 mm/min. Dumbbell-shaped DNA plastic samples (2 mm × 6 mm × 1.5 mm) were cut by using a standard die cutter.

Fracture Toughness Measurement. Single Edge Notch Bending (SENB) test was conducted using a universal testing machine (Instron 5965). The specimen was placed horizontally on the support fixture, and a 100 N load cell was used to record the load. The span was set to 12 mm, and the load was applied at a constant rate of 0.04 mm/min. During the test, a high-speed camera recorded the crack propagation behavior. The dimensions of the single-edge notched

https://doi.org/10.1021/cbe.4c00190
Chem Bio Eng. 2025, 2, 303−311

DNA plastic beams were 15 mm × 3 mm × 1.5 mm. The beams were notched by a diamond blade notch and then polished with a razor blade perpendicular to the lamellar direction. The notch was approximately half the width of the specimens.

Recyclability and Biodegradability of DNA Plastics. DNA plastics were dissolved in deionized water and then lyophilized to obtain DNA powder. DNA solutions of the desired concentration were prepared as needed. The recyclable DNA plastics were prepared through steps, including bidirectional freezing, water vapor annealing, and compression. For biodegradation experiments, the DNA plastics were immersed in an aqueous solution containing DNase I (5 U/μL) at room temperature, and their morphological changes were recorded through optical photographs. The biodegradability of the DNA plastics was further verified by gel electrophoresis.

■ ASSOCIATED CONTENT

Supporting Information

The Supporting Information is available free of charge at https://pubs.acs.org/doi/10.1021/cbe.4c00190.

Polarized image of BFA and FI DNA plastics at different angles; result curves of DNA plastic FI and BFA ⊥ by cyclic loading−unloading experiments; elastic contributions (J_{el}) and plastic contributions (J_{pl}) as functions of crack extension length for FI, BFA ⊥ and BFA ∥; and toughness formulas for DNA plastics based on SENB tests (PDF)

Movie of SENB tests for FI specimen (MP4)

Movie of SENB tests for BFA ⊥ specimen (MP4)

Movie of SENB tests for BFA ∥ specimen (MP4)

■ AUTHOR INFORMATION

Corresponding Authors

Taolin Sun − *South China Advanced Institute for Soft Matter Science and Technology, School of Emergent Soft Matter, South China University of Technology, Guangzhou 510640, China; Guangdong Provincial Key Laboratory of Functional and Intelligent Hybrid Materials and Devices and Guangdong Basic Research Center of Excellence for Energy and Information Polymer Materials, South China University of Technology, Guangzhou 510640, China; State Key Laboratory of Pulp and Paper Engineering, South China University of Technology, Guangzhou, Guangzhou 510640, China;* orcid.org/0000-0001-6006-5859; Email: suntl@scut.edu.cn

Tingjian Chen − *MOE International Joint Research Laboratory on Synthetic Biology and Medicines, School of Biology and Biological Engineering, South China University of Technology, 510006 Guangzhou, China;* orcid.org/0000-0002-4458-4269; Email: chentj@scut.edu.cn

Authors

Xiaofeng Li − *South China Advanced Institute for Soft Matter Science and Technology, School of Emergent Soft Matter, South China University of Technology, Guangzhou 510640, China; Guangdong Provincial Key Laboratory of Functional and Intelligent Hybrid Materials and Devices, South China University of Technology, Guangzhou 510640, China*

Xi Shan − *South China Advanced Institute for Soft Matter Science and Technology, School of Emergent Soft Matter, South China University of Technology, Guangzhou 510640, China; Guangdong Provincial Key Laboratory of Functional and Intelligent Hybrid Materials and Devices, South China University of Technology, Guangzhou 510640, China*

Jiadong Chen − *South China Advanced Institute for Soft Matter Science and Technology, School of Emergent Soft Matter, South China University of Technology, Guangzhou 510640, China; Guangdong Provincial Key Laboratory of Functional and Intelligent Hybrid Materials and Devices, South China University of Technology, Guangzhou 510640, China*

Jun Zhu − *South China Advanced Institute for Soft Matter Science and Technology, School of Emergent Soft Matter, South China University of Technology, Guangzhou 510640, China; Guangdong Provincial Key Laboratory of Functional and Intelligent Hybrid Materials and Devices, South China University of Technology, Guangzhou 510640, China*

Yang Chen − *South China Advanced Institute for Soft Matter Science and Technology, School of Emergent Soft Matter, South China University of Technology, Guangzhou 510640, China; Guangdong Provincial Key Laboratory of Functional and Intelligent Hybrid Materials and Devices, South China University of Technology, Guangzhou 510640, China*

Xueyi Chen − *MOE International Joint Research Laboratory on Synthetic Biology and Medicines, School of Biology and Biological Engineering, South China University of Technology, 510006 Guangzhou, China;* orcid.org/0009-0008-2948-2054

Shahao Li − *South China Advanced Institute for Soft Matter Science and Technology, School of Emergent Soft Matter, South China University of Technology, Guangzhou 510640, China; Guangdong Provincial Key Laboratory of Functional and Intelligent Hybrid Materials and Devices, South China University of Technology, Guangzhou 510640, China*

Mengze Lu − *South China Advanced Institute for Soft Matter Science and Technology, School of Emergent Soft Matter, South China University of Technology, Guangzhou 510640, China; Guangdong Provincial Key Laboratory of Functional and Intelligent Hybrid Materials and Devices, South China University of Technology, Guangzhou 510640, China;* orcid.org/0000-0002-8012-2942

Yuhui Du − *MOE International Joint Research Laboratory on Synthetic Biology and Medicines, School of Biology and Biological Engineering, South China University of Technology, 510006 Guangzhou, China;* orcid.org/0000-0002-2036-5408

Panchao Yin − *South China Advanced Institute for Soft Matter Science and Technology, School of Emergent Soft Matter, South China University of Technology, Guangzhou 510640, China; Guangdong Provincial Key Laboratory of Functional and Intelligent Hybrid Materials and Devices, South China University of Technology, Guangzhou 510640, China;* orcid.org/0000-0003-2902-8376

Complete contact information is available at: https://pubs.acs.org/10.1021/cbe.4c00190

Notes

The authors declare no competing financial interest.

■ ACKNOWLEDGMENTS

This research was supported by the Natural Science Foundation of Guangdong Province (No. 2023A1515012049), Major Program of National Natural Science Foundation of China (Grant No. 11932007), National Natural Science Foundation of China (Grant No. 11972011), Guangdong Provincial Key Laboratory of Functional and

Intelligent Hybrid Materials and Devices (No. 2019B121203003), and the Program for Guangdong Introducing Innovative and Entrepreneurial Teams (2019ZT08Y318), China.

REFERENCES

(1) Schyns, Z. O. G.; Shaver, M. P. Mechanical Recycling of Packaging Plastics: A Review. *Macromol. Rapid Commun.* **2021**, *42* (3), 2000415.
(2) Kaltenbrunner, M.; Sekitani, T.; Reeder, J.; Yokota, T.; Kuribara, K.; Tokuhara, T.; Drack, M.; Schwödiauer, R.; Graz, I.; Bauer-Gogonea, S.; Bauer, S.; Someya, T. An Ultra-Lightweight Design for Imperceptible Plastic Electronics. *Nature* **2013**, *499* (7459), 458−463.
(3) Patil, A.; Patel, A.; Purohit, R. An Overview of Polymeric Materials for Automotive Applications. *Mater. Today: Proc.* **2017**, *4* (2), 3807−3815.
(4) Quan, D.; Bologna, F.; Scarselli, G.; Ivankovic, A.; Murphy, N. Interlaminar Fracture Toughness of Aerospace-Grade Carbon Fibre Reinforced Plastics Interleaved with Thermoplastic Veils. *Composites, Part A* **2020**, *128*, 105642.
(5) Joseph, B.; James, J.; Kalarikkal, N.; Thomas, S. Recycling of Medical Plastics. *Adv. Ind. Eng. Polym. Res.* **2021**, *4* (3), 199−208.
(6) Lambert, S.; Wagner, M. Environmental Performance of Bio-Based and Biodegradable Plastics: the Road Ahead. *Chem. Soc. Rev.* **2017**, *46* (22), 6855−6871.
(7) MacLeod, M.; Arp, H. P. H.; Tekman, M. B.; Jahnke, A. The Global Threat from Plastic Pollution. *Science* **2021**, *373* (6550), 61−65.
(8) Sudesh, K.; Iwata, T. Sustainability of Biobased and Biodegradable Plastics. *Clean: Soil, Air, Water* **2008**, *36* (5−6), 433−442.
(9) Zhao, X.; Wang, Y.; Chen, X.; Yu, X.; Li, W.; Zhang, S.; Meng, X.; Zhao, Z.-M.; Dong, T.; Anderson, A.; Aiyedun, A.; Li, Y.; Webb, E.; Wu, Z.; Kunc, V.; Ragauskas, A.; Ozcan, S.; Zhu, H. Sustainable Bioplastics Derived from Renewable Natural Resources for Food Packaging. *Matter* **2023**, *6* (1), 97−127.
(10) Xie, D.; Zhang, R.; Song, S.; Yang, S.; Yang, A.; Zhang, C.; Song, Y. Nacre-Inspired Starch-Based Bioplastic with Excellent Mechanical Strength and Electromagnetic Interference Shielding. *Carbohydr. Polym.* **2024**, *331*, 121888.
(11) Xia, Q.; Chen, C.; Yao, Y.; Li, J.; He, S.; Zhou, Y.; Li, T.; Pan, X.; Yao, Y.; Hu, L. A Strong, Biodegradable and Recyclable Lignocellulosic Bioplastic. *Nat. Sustain.* **2021**, *4* (7), 627−635.
(12) Priyadarshi, R.; Rhim, J.-W. Chitosan-Based Biodegradable Functional Films for Food Packaging Applications. *Innovative Food Sci. Emerging Technol.* **2020**, *62*, 102346.
(13) Han, J.; Guo, Y.; Wang, H.; Zhang, K.; Yang, D. Sustainable Bioplastic Made from Biomass DNA and Ionomers. *J. Am. Chem. Soc.* **2021**, *143* (46), 19486−19497.
(14) Ji, Y.; Kim, T.; Han, D.; Lee, J. B. Self-Healing and Thermal Responsive DNA Bioplastics for On-Demand Degradable Medical Devices. *ACS Mater. Lett.* **2024**, *6* (4), 1277−1287.
(15) Yamada, M.; Kawamura, M.; Yamada, T. Preparation of Bioplastic Consisting of Salmon Milt DNA. *Sci. Rep.* **2022**, *12* (1), 7423.
(16) Wang, D.; Cui, J.; Gan, M.; Xue, Z.; Wang, J.; Liu, P.; Hu, Y.; Pardo, Y.; Hamada, S.; Yang, D.; Luo, D. Transformation of Biomass DNA into Biodegradable Materials from Gels to Plastics for Reducing Petrochemical Consumption. *J. Am. Chem. Soc.* **2020**, *142* (22), 10114−10124.
(17) Meng, Y.; Zhu, Y.; Zhou, L.; Meng, X.; Yang, Y.; Zhao, R.; Xia, J.; Yang, B.; Lu, Y.; Wu, H.; Mao, L.; Yu, S. Artificial Nacre with High Toughness Amplification Factor: Residual Stress-Engineering Sparks Enhanced Extrinsic Toughening Mechanisms. *Adv. Mater.* **2022**, *34* (9), 2108267.
(18) Bouville, F.; Maire, E.; Meille, S.; Van de Moortèle, B.; Stevenson, A. J.; Deville, S. Strong, Tough and Stiff Bioinspired Ceramics from Brittle Constituents. *Nat. Mater.* **2014**, *13* (5), 508−514.
(19) Mao, L.; Gao, H.; Yao, H.; Liu, L.; Cölfen, H.; Liu, G.; Chen, S.; Li, S.; Yan, Y.; Liu, Y.; Yu, S. Synthetic Nacre by Predesigned Matrix-Directed Mineralization. *Science* **2016**, *354* (6308), 107−110.
(20) Green, M. R.; Sambrook, J. Isolation of High-Molecular-Weight DNA Using Organic Solvents. *Cold Spring Harbor Protocols* **2017**, 356−359.
(21) Burton, K. A Study of the Conditions and Mechanism of the Diphenylamine Reaction for the Colorimetric Estimation of Deoxyribonucleic Acid. *Biochem. J.* **1956**, *62* (2), 315−323.
(22) Hassan, R.; Husin, A.; Sulong, S.; Yusoff, S.; Johan, M. F.; Yahaya, B. H.; Ang, C. Y.; Ghazali, S.; Cheong, S. K. Guidelines for Nucleic Acid Detection and Analysis in Hematological Disorders. *Malays. J. Pathol.* **2015**, *37* (2), 165−173.
(23) Bai, H.; Walsh, F.; Gludovatz, B.; Delattre, B.; Huang, C.; Chen, Y.; Tomsia, A. P.; Ritchie, R. O. Bioinspired Hydroxyapatite/Poly (Methyl Methacrylate) Composite with a Nacre-Mimetic Architecture by a Bidirectional Freezing Method. *Adv. Mater.* **2016**, *28* (1), 50−56.
(24) Bai, H.; Chen, Y.; Delattre, B.; Tomsia, A. P.; Ritchie, R. O. Bioinspired Large-Scale Aligned Porous Materials Assembled with Dual Temperature Gradients. *Sci. Adv.* **2015**, *1* (11), No. e1500849.
(25) Wegst, U. G.; Bai, H.; Saiz, E.; Tomsia, A. P.; Ritchie, R. O. Bioinspired Structural Materials. *Nat. Mater.* **2015**, *14* (1), 23−36.
(26) Xu, Z.; Wu, M.; Gao, W.; Bai, H. A Sustainable Single-Component "Silk Nacre". *Sci. Adv.* **2022**, *8*, No. eabo0946.
(27) Wang, H.; Lu, R.; Yan, J.; Peng, J.; Tomsia, A. P.; Liang, R.; Sun, G.; Liu, M.; Jiang, L.; Cheng, Q. Tough and Conductive Nacre-Inspired MXene/Epoxy Layered Bulk Nanocomposites. *Angew. Chem., Int. Ed.* **2023**, *62* (9), No. e202216874.
(28) Yue, X.; Yang, H.; Han, Z.; Lu, Y.; Yin, C.; Zhao, X.; Liu, Z.; Guan, Q.; Yu, S. Tough and Moldable Sustainable Cellulose-Based Structural Materials via Multiscale Interface Engineering. *Adv. Mater.* **2024**, *36* (7), 2306451.
(29) Aliha, M.; Bahmani, A.; Akhondi, S. Mixed Mode Fracture Toughness Testing of PMMA with Different Three-Point Bend Type Specimens. *Eur. J. Mech. A/Solids* **2016**, *58*, 148−162.
(30) Susanti, C. M. E.; Nakao, T.; Yoshihara, H. Examination of the Failure Behaviour of Wood with a Short Crack in the Tangential-Radial System by Single-Edge-Notched Bending Test. *Eng. Fract. Mech.* **2010**, *77* (13), 2527−2536.
(31) Li, Z.; Wang, R.; Young, R. J.; Deng, L.; Yang, F.; Hao, L.; Jiao, W.; Liu, W. Control of the Functionality of Graphene Oxide for its Application in Epoxy Nanocomposites. *Polymer* **2013**, *54* (23), 6437−6446.
(32) Zioupos, P.; Currey, J. Changes in the Stiffness, Strength, and Toughness of Human Cortical Bone with Age. *Bone* **1998**, *22* (1), 57−66.
(33) Barthelat, F.; Espinosa, H. An Experimental Investigation of Deformation and Fracture of Nacre-Mother of Pearl. *Exp. Mech.* **2007**, *47*, 311−324.
(34) Gao, H.; Chen, S.; Mao, L.; Song, Z.; Yao, H.; Cölfen, H.; Luo, X.; Zhang, F.; Pan, Z.; Meng, Y.; Ni, Y.; Yu, S. Mass Production of Bulk Artificial Nacre with Excellent Mechanical Properties. *Nat. Commun.* **2017**, *8* (1), 287.
(35) Song, J.; Fan, C.; Ma, H.; Liang, L.; Wei, Y. Crack Deflection Occurs by Constrained Microcracking in Nacre. *Acta Mech. Sin.* **2018**, *34*, 143−150.
(36) Al-Maskari, N. S.; McAdams, D. A.; Reddy, J. N. Modeling of a Biological Material Nacre: Waviness Toughness Model. *Mech. Adv. Mater. Struct.* **2019**, *26* (9), 789−795.
(37) Zhao, Y.; Zheng, J.; Xiong, Y.; Wang, H.; Yang, S.; Sun, X.; Zhao, L.; Mikos, A. G.; Wang, X. Hierarchically Engineered Artificial Lamellar Bone with High Strength and Toughness. *Small Struct.* **2023**, *4* (3), 2200256.

https://doi.org/10.1021/cbe.4c00190
Chem Bio Eng. 2025, 2, 303−311